Enhancement of elastic wave energy harvesting using adaptive piezo-lens

Kaijun Yi, Manuel Collet, Simon Chesné, Mélodie Monteil

Enhancement of elastic wave energy harvesting using adaptive piezo-lens

K. Yi [a], M. Collet [a,*], S. Chesne [b], M. Monteil [b]

[a] *LTDS UMR5513 Ecole Centrale de Lyon, 36 Avenue Guy de Collongue, 69130 Ecully, France*
[b] *Université de Lyon, CNRS INSA-Lyon, LaMCoS UMR5259, F-69621 Villeurbanne, France*

This paper exploits an adaptive piezo-lens to improve the harvested power (energy) from traveling waves. The piezo-lens comprises a host plate and piezoelectric patches bonded on the plate surfaces. The piezoelectric patches are shunted with negative capacitance (NC) circuits. The spatial variation of the refractive index inside the piezo-lens domain is designed to fulfill a hyperbolic secant function by tuning the NC values. This design allows the piezo-lens to continuously bend the incident waves toward a designed focal point, resulting in an energy concentration zone with a high level of energy density. This energy concentration effect may be exploited to improve the harvested power from waves. In addition, the piezo-lens is tunable - the waves can be focused at different locations by designing the NC values. This tunability may make the harvesting systems incorporating a piezo-lens be adaptable to environment changes. The above expected practical interests of the piezo-lens for wave energy harvesting are discussed and verified in the paper. Fully coupled numerical models are developed to predict the dynamical responses of the piezoelectric systems.

1. Introduction

Small electronic devices are increasingly employed in many applications in the aerospace, transport and civil engineering fields. Such devices typically require continuous low power supply [1]. This fact motivates massive researches dedicated to the transformation of ambient energy into electricity. Due to the ubiquitous presence of vibration in structures, extensive efforts have been made to harvest vibration energy through piezoelectric, electromagnetic and electrostatic transducers [2]. In practical applications, vibration levels can be low [3] and the vibration energy is typically distributed over a broad frequency band, consequently a lot of these researches were dedicated to obtain higher harvesting efficiency and to extend the operating frequency band of the harvesting system. Examples include (i) tuning the harvesting system through passive or active methods to match the operating frequency with the environment [3,4]; (ii) exploiting nonlinear mechanical mechanisms to widen the operating frequency band [5] or nonlinear circuits to improve the extracted power from the transducers [6–14]; (iii) using phononic crystals [15], metamaterials [16] or acoustic black holes [17] to increase energy densities near the harvesters.

Harvesting vibration energy in structures is well studied, however limited effort has been devoted to harvest energy from traveling waves. Harvesting traveling wave energy is important when built-up structures are involved. In a built-up

* Corresponding author.
E-mail address: manuel.collet@ec-lyon.fr (M. Collet).

structure, the mechanical power transmits from one component to another in the form of traveling waves especially at higher frequency bands [18,19]. Due to the wave propagation, the mechanical energy is distributed in the whole structure with quite low energy densities everywhere. Therefore, the level of the harvested energy from waves could be very low.

In recent years, several innovative harvesting systems have been developed to increase harvested energy from traveling waves. The fundamental idea is to steer waves to increase the energy densities at particular positions and harvest there. Therefore, these systems not only include transducers with connected circuits, but also include structures used to enhance the energy density. The first examples use an elliptical acoustic mirror [20,21] or a parabolic acoustic mirror [22] to focus propagating waves near a specific point. The others are mainly based on metamaterials. Examples include using a defect in an artificial periodic array to localize energy at specific frequencies or building an acoustic funnel formed by arrays of acoustic scatters to guide waves into a narrow channel [22]; exploiting a gradient-index phononic crystal lens to focus waves [23]. However, all these systems are based on unadaptable wave steering methods, they have no ability to adjust themselves to the environment.

Different from the aforementioned methods to steer waves, recently an adaptive piezo-lens is proposed to focus waves [24]. The piezo-lens is designed based on a gradient index medium concept [25]. It is obtained by periodically bonding piezoelectric patches on the surfaces of a host plate. These patches are shunted with negative capacitance (NC) circuits. The NC values are delicately designed to obtain a hyperbolic secant profile of the effective refractive index inside the piezo-lens. Results show that the piezo-lens can focus flexural waves near a designed point in a broad frequency band, and the piezo-lens has the ability to focus waves at different locations by just tuning the NC values. All these qualities make the piezo-lens a potential candidate to develop advanced harvesting systems for waves.

In this paper, a novel system is proposed for improving energy harvesting from traveling waves. This system is composed of a piezo-lens to focus waves and a harvester to yield energy from the focused waves. An analytical relationship which connects the effective refractive index of piezoelectric system to the shunting NC value is developed to design the piezo-lens. Fully coupled finite element models of the piezoelectric systems are developed to predict the dynamic responses. With these tools, we will study the focusing effects and adaptive capability of the piezo-lens, and how can these qualities be exploited to improve the harvesting performances.

2. Piezo-lens for wave focusing

The concept and designing process of the piezo-lens are introduced in this section. The piezo-lens is obtained by periodically bonding piezoelectric patches on the surfaces of a host aluminum plate in a collocated fashion, as depicted in Fig. 1(a). The host plate is lying in the $x-y$ plane and occupying the spatial region $-h_b/2 \leqslant z \leqslant h_b/2$. The piezo-lens zone could be divided into a 14-by-6 array of piezoelectric cell, the patches in each of these cells are shunted with a NC circuit, as shown in Fig. 2.

To focus flexural waves, the refractive indexes of flexural wave inside the piezo-lens zone are designed to fulfill a hyperbolic secant function:

$$n(y) = n_0 \cdot \operatorname{sech}(\alpha(y-\beta)) \tag{1}$$

in which, n_0 represents the refractive index of the background plate, α is the gradient coefficient and β represents the y coordinate of the symmetry axis of the refractive index profile, as illustrated in Fig. 1(b). Due to this design, waves incident into the lens from the Ox direction will be focused at a focal point at the $y=\beta$ line, with a focal length $f=\pi/2\alpha$ measuring from the left boundary of the lens [25]. It should be noted that the piezo-lens is primarily designed for waves from the Ox direc-

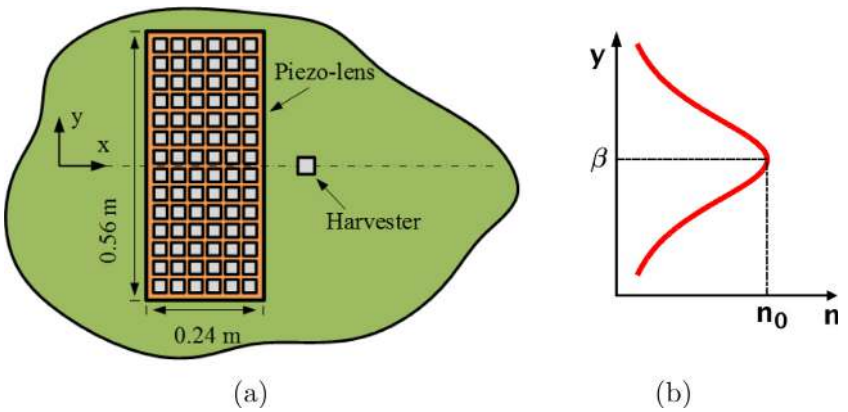

Fig. 1. (a) The harvesting system with piezo-lens and (b) the gradient variation profile of the refractive index $n(y)$.

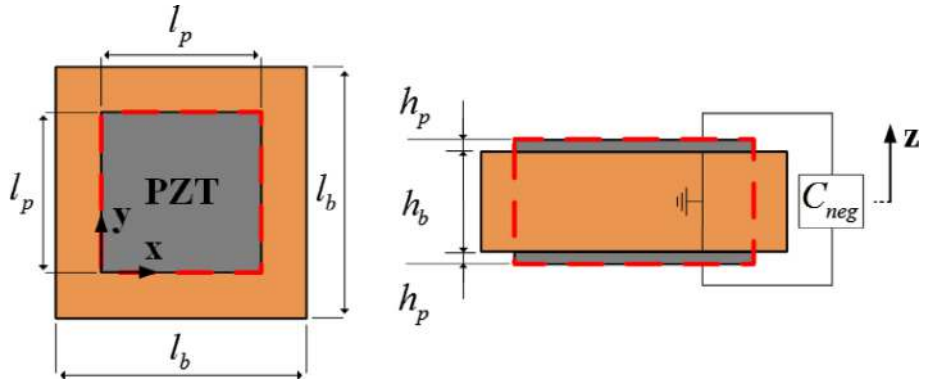

Fig. 2. Top and side view of one unit shunted piezoelectric cell.

tion, and when the waves are incident into the lens from an oblique direction, they will be focused away from the designed focal point [24].

As the effective refractive index of the piezoelectric cell depicted in Fig. 2 can be modified by tuning the shunting NC value [24], its variation inside the piezo-lens is approximately realized in a piecewise form by designing the NC values of cells at different positions. According to Eq. (1), the refractive index only varies in the y direction. Thus, in a piezo-lens, the shunting NC values are equal in a same row (the x direction) but will be different in a same column (the y direction). To determine the required shunting NC value in each row, an analytical relationship between the effective refractive index of the cell and the NC value is developed.

The relationship is obtained in four steps. In the first step, the effective Young's modulus and effective Poisson's ratio of the piezoelectric patches shunted with NC are represented as functions of the NC value:

$$\begin{aligned} E_p &= E_p^{sh}\frac{C_{neg}+C_p^T}{C_{neg}+C_p^T\left(1-k_{31}^2\right)} \\ \mu_p &= \mu_p^{sh}\frac{C_{neg}+C_p^T\left(1+k_{31}^2/\mu_p^{sh}\right)}{C_{neg}+C_p^T\left(1-k_{31}^2\right)} \end{aligned} \tag{2}$$

here, E_p^{sh} and μ_p^{sh} are the Young's modulus and the Poisson's ratio of the short-circuit piezoelectric material, respectively; k_{31} is the coupling factor; C_p^T is the free intrinsic capacitance (namely the capacitance when the patch is under constant stress); C_{neg} is the applied NC value.

In the second step, the effective parameters of the shunted piezoelectric sandwich structure highlighted by the dashed lines in Fig. 2 are determined according to the classical laminated plate theory [26]. The effective area density and effective flexural rigidity of the piezoelectric sandwich structure are expressed as:

$$\begin{aligned} \rho_A &= \rho_b h_b + 2\rho_p h_p \\ D_A &= D_b + \frac{2E_p}{3(1-\mu_p^2)}\left[\left(\frac{h_b}{2}+h_p\right)^3-\left(\frac{h_b}{2}\right)^3\right] \end{aligned} \tag{3}$$

here, $D_b=\frac{E_b h_b^3}{12\left(1-\mu_b^2\right)}$ is the flexural rigidity of the host plate and E_b, μ_b denote the Young's modulus and the Poisson's ratio of the host plate respectively; ρ_b and ρ_p are the densities of the host plate and the piezoelectric patches respectively.

In the third step, the effective area density and effective flexural rigidity of the entire shunted piezoelectric cell are derived, they are expressed as [27]:

$$\begin{aligned} \rho_{eff} &= \chi\rho_A + (1-\chi)\rho_b h_b \\ D_{eff} &= \frac{D_A D_b}{\chi D_A + (1-\chi)D_b} \end{aligned} \tag{4}$$

here, $\chi=(l_p/l_b)^2$ is the ratio of the surface area covered by a piezoelectric patch to the surface area of a unit cell.

In the last step, the effective refractive index of flexural wave incident from the background plate into the shunted piezoelectric cell is obtained:

$$n_{eff} = \left(\frac{\rho_{eff}D_b}{\rho_b h_b D_{eff}}\right)^{1/4} \tag{5}$$

With the relationship in Eq. (5), a piezo-lens is designed in three steps. Firstly, the parameters α and β in the refractive index function in Eq. (1) are chosen to design the location of the focal point. Then, the required refractive index for each row of piezoelectric cell in the lens zone is obtained by substituting the central y coordinate of each row into Eq. (1). Lastly, the required refractive index for each row is fulfilled by choosing the NC value according to Eq. (5).

3. Prospect of exploiting piezo-lens in wave energy harvesting

It is demonstrated in [24] that the piezo-lens can concentrate energy inside a limited zone around the designed focal point and the location of this energy concentration zone can be adjusted by tuning the NC values. These two qualities can be of great practical interest for wave energy harvesting. In particular, the pre-designed location of the zone with a high level of energy density identifies the optimal locations for harvesting. Besides, even though the piezo-lens is initially designed to focus waves from the Ox direction, and when the incident direction is changed, waves will be focused away from the designed focal point [24], where the transducer for harvesting is placed; but by exploiting the tunability of the piezo-lens, the location of the energy concentration zone may could be adjusted back to the desired site.

To explore the concept of using piezo-lens in wave energy harvesting, a system incorporating a piezo-lens and a harvester (namely, a harvesting device) is proposed, as illustrated in Fig. 1(a). The harvester is composed of a piezoelectric patch bonded on the upper surface of the plate near the lens (the exact location will be specified in Section 5) and a connected resistor, as illustrated in Fig. 3. In the figure, the piezoelectric patch is equivalently represented by a current source $I_{eq}(t)$ and a capacitance C_h with the value equal to the blocked intrinsic capacitance (i.e. the capacitance when the patch is under constant strain condition) [12]. Since the output $V_h(t)$ of the harvester in Fig. 3 is an AC voltage but most of the real-life electronic devices require DC input, this AC device has limited practical value. However, the amplitude of the dissipated power by the resistor could be used as a metric to estimate the potential power that could be converted and harvested via the piezoelectric transducer. Thus, the AC device is useful in evaluating the performances of harvesting systems especially with complicated mechanical parts and is used in many studies [15,17,20–22,28]. Under harmonic excitations, the amplitudes of the output voltage and harvested power (namely the dissipated power by the resistor) are:

$$\widetilde{V}_h = -j\omega\widetilde{Q}_h R, \quad P = \widetilde{V}_h^2/R \tag{6}$$

$\widetilde{Q}_h$ is the amplitude of charge flowing to the piezoelectric patch.

4. Numerical model

To study the performances of the piezo-lens and the harvesting system, fully coupled finite element (FE) models of piezoelectric systems are developed. The FE models contain a host structure, multiple piezoelectric patches and circuits connected to the patches. Their are obtained in two steps: first, the models for the linear piezoelectric systems are obtained; then, the shunts are connected to the models through particular electrical boundary conditions.

In the FE models, the structures are discretized by 3D quadratic Lagrange elements. Each of the nodes corresponding to the piezoelectric patches has three mechanical degrees of freedom (DOFs) and an electrical potential DOF. The equilibrium equations for the discretized fully coupled piezoelectric system are:

$$\begin{aligned} &\boldsymbol{M}_{dd}\ddot{\boldsymbol{d}} + \boldsymbol{K}_{dd}\boldsymbol{d} + \boldsymbol{K}_{dV}\boldsymbol{V} = \boldsymbol{F} \\ &-\boldsymbol{K}_{dV}^{T}\boldsymbol{d} + \boldsymbol{K}_{VV}\boldsymbol{V} = \boldsymbol{Q} \end{aligned} \tag{7}$$

here, $\boldsymbol{d}$ and $\boldsymbol{V}$ represent the structural and potential DOFs, respectively; $\boldsymbol{F}$ and $\boldsymbol{Q}$ are the mechanical forces and charges respectively.

The equations in (7) are rewritten under following considerations: (i) the potential DOFs in the piezoelectric patches can be partitioned into DOFs inside the patches, DOFs on the free electrodes of the patches and DOFs on the bonding surfaces; (ii) the potential DOFs on the bonding surfaces are grounded, thus the corresponding equations and columns are directly removed; (iii) there is no charge source inside the piezoelectric patches; (iv) in the system, the piezoelectric patches are con-

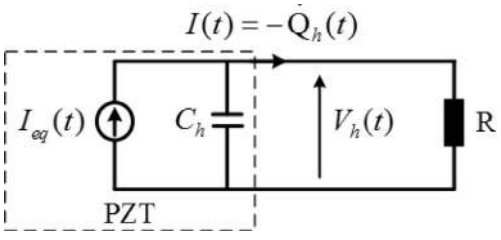

Fig. 3. An AC device.

nected with different circuits - the patches constituting the piezo-lens are connected with NC circuits and the patch for harvesting is connected with resistor, therefore, the DOFs on the free electrodes are further separated into DOFs corresponding to the patches in the piezo-lens and DOFs of the patch for harvesting; (v) as the DOFs on one electrode have identical potentials, the potential DOFs on the free electrode of each piezoelectric patch are reduced such that only one master potential DOF remains on the free electrode per patch. Consequently, the governing equations can be rewritten as below:

$$\begin{bmatrix} \mathbf{M_{dd}} & 0 & 0 & 0 \\ 0 & 0 & 0 & 0 \\ 0 & 0 & 0 & 0 \\ 0 & 0 & 0 & 0 \end{bmatrix} \begin{Bmatrix} \ddot{\boldsymbol{d}} \\ \ddot{\boldsymbol{V}}_i \\ \ddot{\boldsymbol{V}}_L \\ \ddot{\boldsymbol{V}}_h \end{Bmatrix} + \begin{bmatrix} \boldsymbol{K}_{dd} & \mathbf{K}_{di} & \mathbf{K}_{dL} & \mathbf{K}_{dh} \\ -\mathbf{K}_{di}^T & \mathbf{K}_{ii} & \mathbf{K}_{iL} & \mathbf{K}_{ih} \\ -\mathbf{K}_{dL}^T & \mathbf{K}_{iL}^T & \mathbf{K}_{LL} & 0 \\ -\mathbf{K}_{dh}^T & \mathbf{K}_{ih}^T & 0 & \mathbf{K}_{hh} \end{bmatrix} \begin{Bmatrix} \boldsymbol{d} \\ \boldsymbol{V}_i \\ \boldsymbol{V}_L \\ \boldsymbol{V}_h \end{Bmatrix} = \begin{Bmatrix} \boldsymbol{F} \\ 0 \\ \boldsymbol{Q}_L \\ \boldsymbol{Q}_h \end{Bmatrix} \tag{8}$$

here, $\boldsymbol{V}_i$ are the DOFs inside the patches; $\boldsymbol{V}_L, \boldsymbol{V}_h$ are the master DOFs on the free electrodes of the patches in the lens and the patch for harvesting, respectively; $\boldsymbol{Q}_L, \boldsymbol{Q}_h$ are the charges flowing to the patches in the lens and patch for harvesting respectively. More details about above process could be found in [29].

Under harmonic excitations, Eqs. (8) are simplified as:

$$\begin{bmatrix} -\omega^2 \boldsymbol{M}_{dd} + \boldsymbol{K}_{dd} & \mathbf{K}_{di} & \mathbf{K}_{dL} & \mathbf{K}_{dh} \\ -\mathbf{K}_{di}^T & \mathbf{K}_{ii} & \mathbf{K}_{iL} & \mathbf{K}_{ih} \\ -\mathbf{K}_{dL}^T & \mathbf{K}_{iL}^T & \mathbf{K}_{LL} & 0 \\ -\mathbf{K}_{dh}^T & \mathbf{K}_{ih}^T & 0 & \mathbf{K}_{hh} \end{bmatrix} \begin{Bmatrix} \tilde{\boldsymbol{d}} \\ \tilde{\boldsymbol{V}}_i \\ \tilde{\boldsymbol{V}}_L \\ \tilde{\boldsymbol{V}}_h \end{Bmatrix} = \begin{Bmatrix} \tilde{\boldsymbol{F}} \\ 0 \\ \tilde{\boldsymbol{Q}}_L \\ \tilde{\boldsymbol{Q}}_h \end{Bmatrix} \tag{9}$$

the symbol $\tilde{(.)}$ denotes the complex amplitude in the frequency domain.

In the simulations, perfectly matched layer boundaries are used to avoid reflections at the ends of the host plate [30]. The NC circuits are connected into the piezoelectric cells by considering following electrical boundary condition:

$$\tilde{\boldsymbol{Q}}_L = -\boldsymbol{C}_{\boldsymbol{neg}} \tilde{\boldsymbol{V}}_L \tag{10}$$

The AC device in Fig. 3 is introduced into the model through the first relation in Eq. (6).

5. Numerical results

In the numerical studies, the dimensions of the piezo-lens are 0.24 m × 0.58 m, as depicted in Fig. 1(a). The geometry parameters of the piezoelectric cells and piezoelectric patch for harvesting are given in Table 1, meanings of the symbols used in Table 1 are given in Fig. 2. The Young's modulus, Poisson's ratio and density of the aluminum plate are $E_b = 70$ GPa , $\mu_b = 0.3$ and $\rho_b = 2700\ \mathrm{kg/m^3}$, respectively. The material parameters for the PZTs are listed in Table 2. Line harmonic transverse forces are used to generate plane waves. Note that, in the simulations, without further information, the waves are incident into the piezo-lens from the *Ox* direction.

5.1. Focusing effects and adaptive capability of piezo-lens

In Section 3, we made the expectation that the piezo-lens has great practical interests for wave energy harvesting. In this subsection, performances of the piezo-lens are presented and discussed in details to support this prediction. In order to study the effects of the piezo-lens on waves, the total mechanical energy flux $\boldsymbol{I}$ on the cross-section of the host plate is used to indicate the wave paths, it is expressed as:

$$\boldsymbol{I} = \frac{1}{2}\omega \cdot \int_{-\frac{h_b}{2}}^{\frac{h_b}{2}} re(-\boldsymbol{\sigma} \cdot \boldsymbol{w}^*) dz \tag{11}$$

here, $\boldsymbol{\sigma}$ and $\boldsymbol{w}$ are the stress and displacement tensors; $(\cdot)^*$ represents conjugate value and $re(\cdot)$ means only the real part is retained.

In addition, the kinetic energy density E_k in the host plate is used to evaluate the spatial distribution of the energy after the lens, it is obtained as:

$$E_k = \frac{1}{4}\omega^2 \rho_b \boldsymbol{w}^{*T} \cdot \boldsymbol{w} \tag{12}$$

The kinetic energy is connected with the velocities which could be directly measured in the experiments, thus using it rather than the strain energy could facilitate the comparison between the numerical and future experimental results.

To numerically demonstrate the focusing effect, the parameters of the piezo-lens are designed as $\alpha = \pi/0.6$ and $\beta = 0$. With these parameters, the flexural waves incident from the *Ox* direction will be theoretically focused at a point on the central axis of the lens (namely the $y = 0$ line) with a distance of 0.06 m from the right boundary of the lens. Fig. 4 shows the mechanical energy flux and kinetic energy distribution after the lens at 2000 Hz. The arrows in Fig. 4(a) and (b) indicate the propagating directions of the waves. From the comparison, it can be observed that the waves are bended by the piezo-lens

Table 1
Geometry parameters.

	l_b	h_b	l_p	h_p
Piezoelectric cell	0.04 m	0.005 m	0.035 m	0.001 m
Piezoelectric patch for harvesting	\	\	0.05 m	0.001 m

Table 2
Material parameters of PZT26.

Symbol	Value	Property
$S_{11}^E = S_{22}^E, S_{33}^E$	$1.30 \times 10^{-11}, 1.96 \times 10^{-11}$ (Pa^{-1})	Compliance matrix under constant electric field
$S_{12}^E, S_{13}^E = S_{23}^E$	$-4.35 \times 10^{-12}, -7.05 \times 10^{-12}$ (Pa^{-1})	
$S_{44}^E = S_{55}^E, S_{66}^E$	$3.32 \times 10^{-11}, 3.47 \times 10^{-11}$ (Pa^{-1})	
$d_{31} = d_{32}$	-1.28×10^{-10} (C/N)	Piezoelectric matrix
d_{33}	3.28×10^{-10} (C/N)	
$d_{24} = d_{15}$	3.27×10^{-10} (C/N)	
ρ	7700 (kg/m^3)	Density
$\varepsilon_{11}^\sigma = \varepsilon_{22}^\sigma, \varepsilon_{33}^\sigma$	$1190\varepsilon_0, 1330\varepsilon_0$	Dielectric permittivity under constant stress

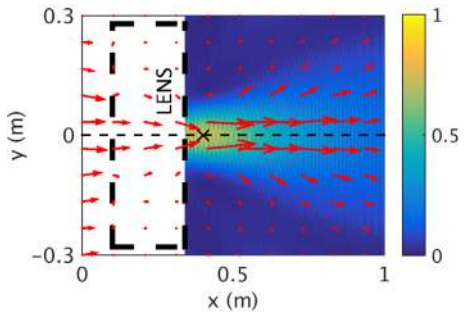

(a) mechanical energy flux in a plate with the piezo-lens

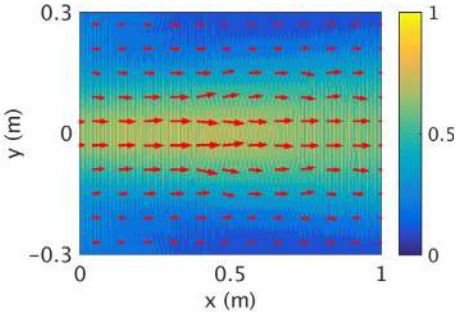

(b) mechanical energy flux in a plate without piezo-lens

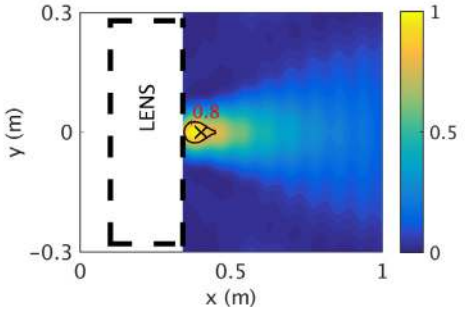

(c) kinetic energy distribution after the lens

Fig. 4. Mechanical energy flux and kinetic energy distribution after the lens at 2000 Hz. The black cross represents the designed focal point, the circle with solid line indicates the energy concentration zone.

toward the designed focal point. Consequently, the energy is concentrated around the focal point. The energy concentration zone, highlighted by a circle with solid line in Fig. 4(c), is used to estimate where most of the energy is concentrated, this zone is defined as:

$$\frac{E_k(x,y)}{max(E_k(x,y))} \geqslant 0.8 \tag{13}$$

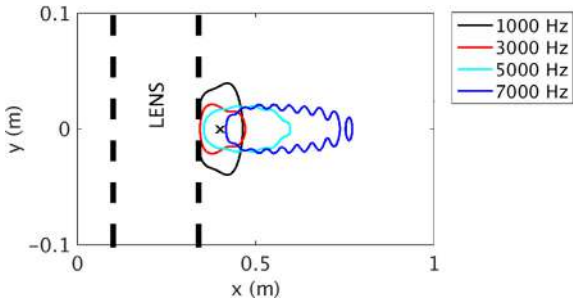

Fig. 5. Energy concentration zones at different frequencies.

in which, $E_k(x,y)$ is the kinetic energy density after the lens. In the context of wave propagation here, high level of kinetic energy density inside the energy concentration zone also means high level of strain energy density [31]. Therefore, harvesting inside the energy concentration zone using piezoelectric transducers may yield more power (energy).

According to the authors' previous work [24], the above demonstrated energy concentration effect can be observed in a large frequency band, and this frequency band is dominated by the geometry parameters of the lens and cell. With the geometry parameters given in Fig. 1(a) and Table 1, the piezo-lens is effective from around 100 Hz to 8000 Hz. Fig. 5 shows the energy concentration zones at different frequencies inside the effective frequency band when the parameters are $\alpha = \pi/0.6$ and $\beta = 0$. It can be seen that at most of the frequencies, the energy is concentrated around the designed focal point. Thus the pre-designed focal point may be an optimal location to put the harvester in order to obtain boosted power in a large frequency band. However it should also be noted that at higher frequencies (e.g. 7000 Hz), the energy concentration zone will shift to the right hand side of the designed focal point. This phenomenon is probably induced by the fact that the wavelength is more comparable to the cell's length at higher frequencies. Specifically, at smaller wavelengths, the variation of refractive index inside the piezo-lens will be less smooth since it is realized in a piecewise form; besides, the homogenized model used in Section 2 will be less accurate [27]. The influences of this shifting phenomenon on the harvesting performance will be addressed in Section 5.2.

Except the energy concentration effect, another remarkable merit of the piezo-lens is its tunability. The spatial variation of the refractive index inside the piezo-lens zone is realized by designing the NC values of the cells at different locations. As the theoretical focal point of the lens is determined by the refractive index profile in the lens, thus by tuning the NC values, different variations of the refractive index could be realized to focus waves at different locations. This adaptability is verified in [24]: by tuning the NC values, the energy can be concentrated at different locations along the x or y directions. It should be noted that as the distance from the focal point to the right boundary or to the central axis of the lens increases, the energy will be less concentrated. Therefore in order to obtain better energy concentration effect, the focal point should be tuned on the central axis and be close to the lens boundary.

The adaptability of the piezo-lens may be exploited to deal with the environment changes. When the piezo-lens is used in the harvesting system depicted in Fig. 1(a), it is primarily designed to focus waves from the Ox direction, the harvester is probably located on the central axis and near the focal point. However, in practice the directions of the incident waves may be changed - the waves may no longer incident from the Ox direction, but from an oblique direction. Due to this modification, the waves are focused away from the originally designed location, as illustrated in Fig. 6(a). Since the harvester is initially located near the designed focal point, the deviation of the energy concentration zone will probably result in significant reduction of the harvested power. The tunability of the piezo-lens could be used to handle this kind of circumstances. When the waves are incident from an oblique direction, the present focal point corresponding to the oblique waves has the same x coordinate but different y coordinate with the designed one, as illustrated in Fig. 6(a) (more details can be found in Section 4.4.1 in [24]). Recalling that the y location of the focal point is connected with the parameter β. Thus in order to adjust the present focal point back to the desired location (namely the originally designed focal point on the central axis), the value of β need to be redesigned to tune the y location of the present focal point. For example, when the waves are incident from the left bottom direction as illustrated in Fig. 6(a), the present focal point is 'above' the desired one (indicated by the cross in the figure). Thus, the value of β need to be decreased to move the present focal point 'down' to the central axis, as illustrated in figures from 6(b)–(d).

5.2. Wave energy harvesting using piezo-lens

The above subsection fully discussed the expected practical interests of piezo-lens for wave energy harvesting. In summary, the results above lead to two major expectations: (i) the designed focal point may be a good choice to place the harvester to obtain boosted power in a wide frequency band; (ii) the tunability of the piezo-lens could be exploited to cope with the change of wave incident direction. These expectations are verified here.

According to the discussions in Section 5.1, the focal point should be designed on the central axis and near the lens boundary to obtain more concentrated energy zone. Thus, the piezo-lens's parameters are chosen as $\alpha = \pi/0.6$ and $\beta = 0$.

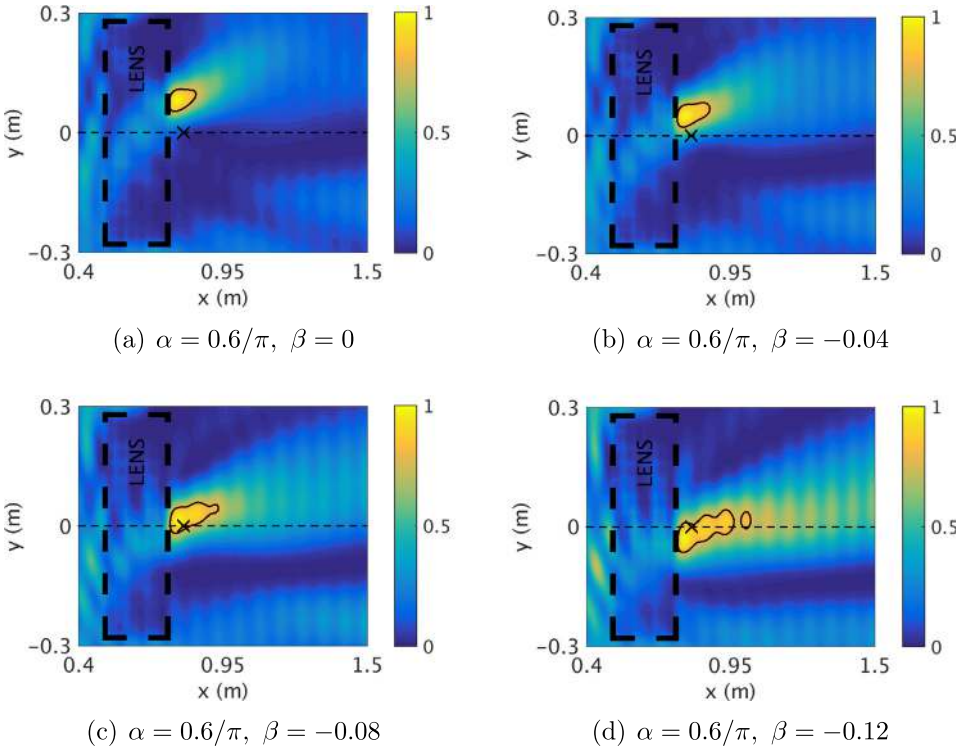

Fig. 6. Adjusting the location of the energy concentration zone when waves are incident from the left bottom direction with an angle equal to 20°. Circles with solid line represent the energy concentration zones; crosses indicate the originally designed focal points.

To demonstrate the first expectation, the harvested power at different frequencies for different load resistances is shown in Fig. 7 when the harvester is mounted at the focal point. In the figure, the maximum harvested power in the case without lens is normalized to unity; only the results at the frequencies from 1000 Hz to 7000 Hz are shown, because the piezo-lens has better performance within this frequency band, as will be seen hereinafter. From Fig. 7, it can be seen that the harvested power is substantially boosted over a wide frequency range when the piezo-lens is applied. To more precisely estimate how many times the power could be improved, a gain ratio is defined as the ratio of the harvested power with piezo-lens to that without lens. Fig. 8(a) shows the gain ratios at different cases. One can point out that the gain ratio is nearly independent of the resistance. Due to this independence, the gain ratios at different frequency could be studied by setting the resistance as a constant value, as depicted in Fig. 8(b). It can be observed that from 1000 Hz to 7000 Hz, the harvested power is more than doubled; particularly at some frequencies, the power is improved over 400% of the one corresponding to the case without lens; below 1000 Hz and above 7000 Hz, the harvested power is barely enhanced or even decreased, this is because the piezo-lens has poor focusing performances at the frequencies close to the lower and upper limits of the effective frequency band [24].

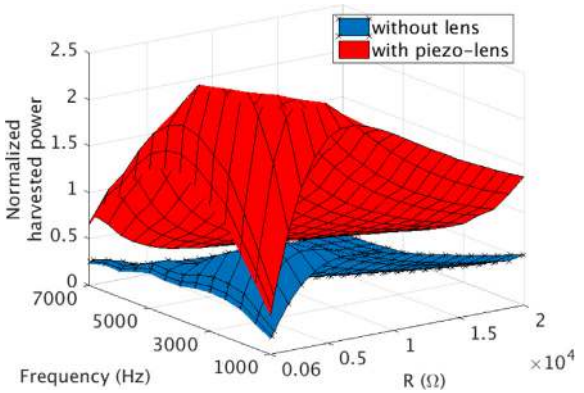

Fig. 7. Harvested power versus resistance and frequency.

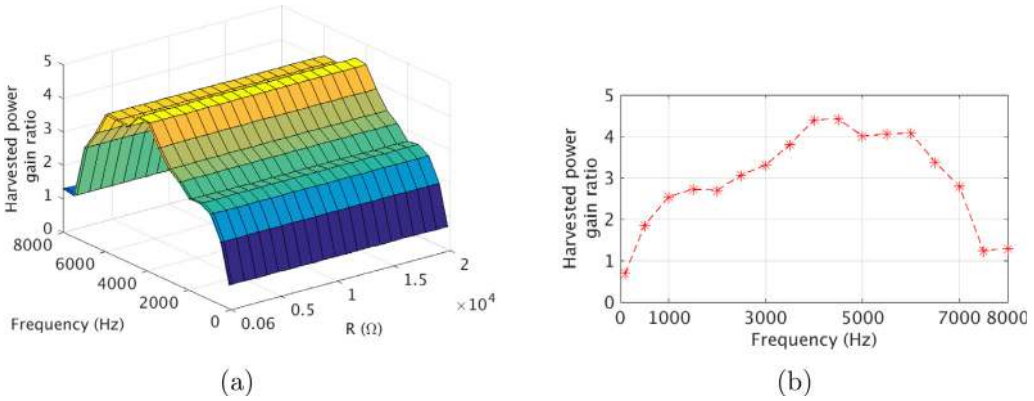

Fig. 8. (a) Gain ratio of harvested power versus frequency and resistance; (b) gain ratio of harvested power versus frequency when $R = 1000\,\Omega$.

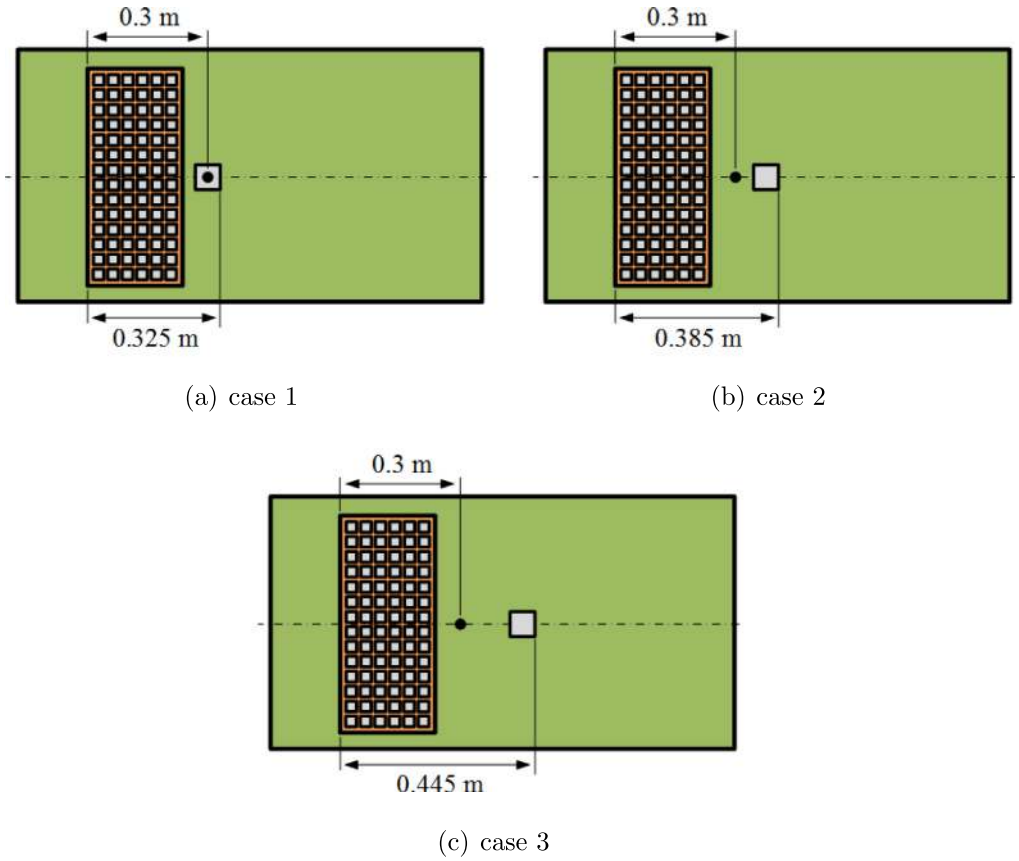

(a) case 1 (b) case 2

(c) case 3

Fig. 9. Harvesting at different positions, the point indicates the designed focal point.

The results above show that harvesting at the focal point can obtain boosted power in a wide frequency band. However as the frequency increases, the energy concentration zone will become longer in the x direction and shift to the right hand side along the central axis of the lens, as shown in Fig. 5, thus harvesting at different sites may lead to diverse harvesting performances, i.e. the focal point may not be the most suitable place to put the harvester. Accordingly, it is important to study the harvesting performances at different locations.

The waves on both sides of the central axis of the piezo-lens are bended toward the axis, due to the symmetry of the lens, these waves meet each other on the central axis with the same phase, thus in the energy concentration zone, locations on the central axis have the highest energy density. Besides, if the harvester is located too far from the focal point (namely is outside

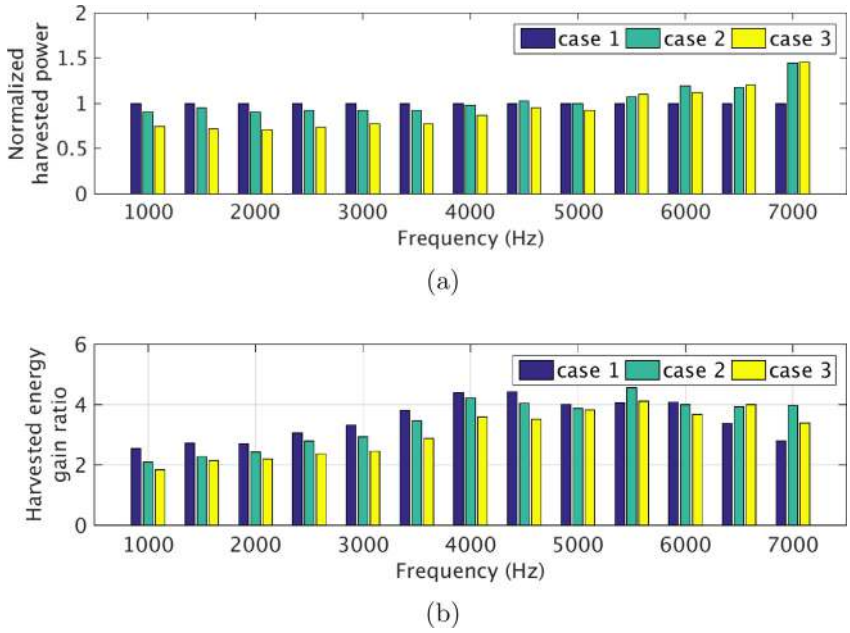

Fig. 10. Comparison of (a) harvested power and (b) gain ratio between different cases when $R = 1000\,\Omega$.

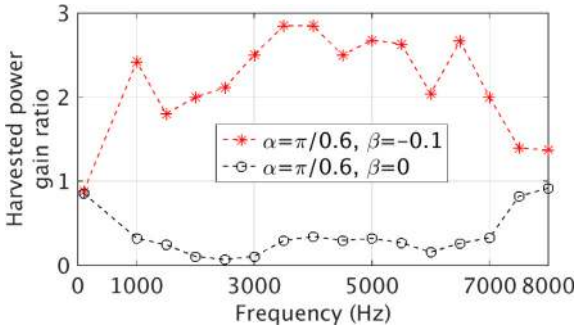

Fig. 11. Gain ratios of harvested power at different frequencies with the original ($\alpha = 0.6/\pi, \beta = 0$) and redesigned ($\alpha = 0.6/\pi, \beta = -0.1$) piezo-lenses. Waves are incident from the left bottom direction with an angle equal to 20° and $R = 1000\,\Omega$.

all the energy concentration zones), the harvesting performance apparently will be poor. Based on these understandings, this part is focused on studying the axial location effect of the harvester. In the studies, three different locations are chosen to put the harvester, as illustrated in Fig. 9. In case 1, the harvester is at the focal point; in case 3, the harvester is outside most of the energy concentration zones but still within the zones corresponding to frequencies larger than 5000 Hz; the harvester in case 2 is placed between the aforementioned two locations. The harvested power and gain ratios of these three cases are compared in Fig. 10, the harvested power of case 1 at each frequency is normalized to unity. As expected, from 1000 Hz to 5000 Hz, case 1 has better performance than case 2 and 3; on contrary, at frequencies above 5000 Hz, case 2 and 3 have better performances. However except at 7000 Hz, the relative differences between the harvested power of these three cases are less than 30%, they are small compared with the gain ratios, which are typically larger than 2 as can be seen in Fig. 10(b). That is to say, harvesting at any of these three locations can yield considerably boosted power in a large frequency band, in other words, even thought the energy concentration zone is shifting with the increasing of frequency, the harvesting is insensitive to the location as long as the harvester is placed on the central axis and is not too far from the focal point. Based on this conclusion and recalling that the focal point is a pre-designed location, it is reasonable to say that the designed focal point is the most suitable place for harvesting.

The second expectation, namely the tunable capability, is verified by the studies presented in this paragraph. In the above researches, the piezo-lens' parameters were initially designed as $\alpha = \pi/0.6, \beta = 0$, and the harvester was mounted at the focal point. It is demonstrated that when the waves are incident from the Ox direction, the piezo-lens can considerably improve the harvested power. Nevertheless, when the directions of waves are changed, the piezo-lens with the parameters

$\alpha = \pi/0.6$ and $\beta = 0$ will focus the waves to the other location instead of the designed focal point (see Fig. 6(a)). Since the harvester is located at the initially designed focal point, and is not inside the current energy concentration zones, the harvested power is significantly reduced, as can be observed in Fig. 11. However, due to the adaptability of the piezo-lens, the energy concentration zone could be adjusted back to the location where the harvester is mounted by redesigning the piezo-lens. Thus the harvester could again yield improved power in a large frequency band.

Since the NC circuits in the piezo-lens contain active elements and resistive parts, it is also important to discuss the energy balance of the harvesting system. In the steady state cases, the time-averaged power consumed by the active elements is null. Besides, the dissipated power of the circuit could be tuned to be very small [32]. Meanwhile, we can also use more efficient harvester to improve the harvested power. Thus the harvested power is possible to be significantly larger than the dissipated power.

6. Conclusions

A piezo-lens is explored to improve the harvested power from traveling waves. The piezo-lens is composed of an array of piezoelectric cell shunted with NC circuit. The spatial variation of the refractive index inside the lens zone is designed to fulfill a hyperbolic secant function by tuning the NC values of cells at different locations. With this design, the piezo-lens will bend the incident waves toward a designed focal point, consequently forming a zone with concentrated energy. This energy concentration effect is observed in a large frequency band, from about 100 Hz to 8000 Hz. Due to this broadband energy concentration effect, when a harvester is placed at the designed focal point, the harvested power is considerably improved within the effective frequency band of the lens. It is also observed that as the frequency increases, the energy concentration zone will shift to the right hand side of the designed focal point. However, even though there is this shifting phenomenon, it is demonstrated that the designed focal point is still the most suitable place for harvesting. Except the energy concentration effect, the piezo-lens is also adaptable. By tuning the NC values of the cells composing the piezo-lens, the energy can be focused at different locations. The focal point is recommended to be tuned on the central axis of the lens and near the lens boundary to obtain better energy concentration effect. In addition, the tunability can be exploited to handle the change of wave incident direction. The piezo-lens is initially designed to focus waves from the *Ox* direction. In practice, the waves' direction may be changed. Under these circumstances, the energy is concentrated away from the designed focal point, at where the harvester is placed. Consequently, the harvested power is significantly reduced. However, by tuning the piezo-lens, the energy concentration zone can be adjusted back to the desired location to improve the harvested power. In the next step of this program, experiments will be done to validate the results in this paper and to fully analyze the energy balance of the harvesting system.

Acknowledgement

The authors acknowledge Carnot Institute Ingénierie@Lyon for granting this study. The first author also thanks a scholarship provided by the China Scholarship Council to pursue his doctorate in France.

References

[1] Zhongsheng Chen, Bin Guo, Yongmin Yang, Congcong Cheng, Metamaterials-based enhanced energy harvesting: a review, Phys. B: Condens. Matter 438 (2014) 1–8.
[2] Minh Quyen Le, Jean-Fabien Capsal, Mickaël Lallart, Yoann Hebrard, Andre Van Der Ham, Nicolas Reffe, Lionel Geynet, Pierre-Jean Cottinet, Review on energy harvesting for structural health monitoring in aeronautical applications, Prog. Aerosp. Sci. 79 (2015) 1–11.
[3] Dibin Zhu, John Tudor, Steve Stephen P. Beeby, Michael J. Tudor, Steve Stephen P. Beeby, Strategies for increasing the operating frequency range of vibration energy harvesters: a review, Meas. Sci. Technol. 21 (2) (2010) 022001.
[4] N. Jackson, F. Stam, O.Z. Olszewski, H. Doyle, A. Quinn, A. Mathewson, Widening the bandwidth of vibration energy harvesters using a liquid-based non-uniform load distribution, Sens. Actuat. A: Phys. 246 (2016) 170–179.
[5] Liuyang Xiong, Lihua Tang, Brian R. Mace, Internal resonance with commensurability induced by an auxiliary oscillator for broadband energy harvesting, Appl. Phys. Lett. 108 (20) (2016) 203901.
[6] Daniel Guyomar, Adrien Badel, Elie Lefeuvre, Claude Richard, Toward energy harvesting using active materials and conversion improvement by nonlinear processing, IEEE Trans. Ultrason. Ferroelectr. Freq. Contr. 52 (4) (2005) 584–594.
[7] E. Lefeuvre, A. Badel, C. Richard, L. Petit, D. Guyomar, A comparison between several vibration-powered piezoelectric generators for standalone systems, Sens. Actuat. A: Phys. 126 (2) (2006) 405–416.
[8] Y.C. Shu, I.C. Lien, W.J. Wu, An improved analysis of the SSHI interface in piezoelectric energy harvesting, Smart Mater. Struct. 16 (6) (2007) 2253–2264.
[9] Mickaël Lallart, Lauric Garbuio, Lionel Petit, Claude Richard, Daniel Guyomar, Double synchronized switch harvesting (DSSH): a new energy harvesting scheme for efficient energy extraction, IEEE Trans. Ultrason. Ferroelectr. Freq. Contr. 55 (10) (2008) 2119–2130.
[10] I.C. Lien, Y.C. Shu, W.J. Wu, S.M. Shiu, H.C. Lin, Revisit of series-SSHI with comparisons to other interfacing circuits in piezoelectric energy harvesting, Smart Mater. Struct. 19 (12) (2010) 125009.
[11] Hui Shen, Jinhao Qiu, Hongli Ji, Kongjun Zhu, Marco Balsi, Enhanced synchronized switch harvesting: a new energy harvesting scheme for efficient energy extraction, Smart Mater. Struct. 19 (11) (2010) 115017.
[12] Junrui Liang, Wei-hsin Liao, Energy flow in piezoelectric energy harvesting systems, Smart Mater. Struct. 20 (1) (2011) 015005.
[13] Daniel Guyomar, Mickaël Lallart, Recent progress in piezoelectric conversion and energy harvesting using nonlinear electronic interfaces and issues in small scale implementation, Micromachines 2 (2) (2011) 274–294.
[14] Hui Shen, Hongli Ji, Jinhao Qiu, Yixiang Bian, Dawei Liu, Adaptive synchronized switch harvesting: a new piezoelectric energy harvesting scheme for wideband vibrations, Sens. Actuat. A: Phys. 226 (2015) 21–36.
[15] Zhongsheng Chen, Yongmin Yang, Zhimiao Lu, Yanting Luo, Broadband characteristics of vibration energy harvesting using one-dimensional phononic piezoelectric cantilever beams, Phys. B: Condens. Matter 410 (1) (2013) 5–12.

[16] Y. Fan, M. Collet, M. Ichchou, L. Li, O. Bareille, Z. Dimitrijevic, A wave-based design of semi-active piezoelectric composites for broadband vibration control, Smart Mater. Struct. 25 (5) (2016) 055032.
[17] Liuxian Zhao, Stephen C. Conlon, Fabio Semperlotti, Broadband energy harvesting using acoustic black hole structural tailoring, Smart Mater. Struct. 23 (6) (2014) 065021.
[18] H.G.D. Goyder, R.G. White, Vibrational power flow from machines into built-up structures, Part I: Introduction and approximate analyses of beam and plate-like foundations, J. Sound Vib. 68 (1) (1980) 59–75.
[19] Y. Fan, M. Collet, M. Ichchou, L. Li, O. Bareille, Z. Dimitrijevic, Energy flow prediction in built-up structures through a hybrid finite element/wave and finite element approach, Mech. Syst. Signal Process. 66–67 (May) (2016) 137–158.
[20] M. Carrara, M.R. Cacan, M.J. Leamy, M. Ruzzene, A. Erturk, Dramatic enhancement of structure-borne wave energy harvesting using an elliptical acoustic mirror, Appl. Phys. Lett. 100 (20) (2012) 16–20.
[21] M. Carrara, J.A. Kulpe, S. Leadenham, M.J. Leamy, A. Erturk, Fourier transform-based design of a patterned piezoelectric energy harvester integrated with an elastoacoustic mirror, Appl. Phys. Lett. 106 (1) (2015) 16–20.
[22] M. Carrara, M.R. Cacan, J. Toussaint, M.J. Leamy, M. Ruzzene, A. Erturk, Metamaterial-inspired structures and concepts for elastoacoustic wave energy harvesting, Smart Mater. Struct. 22 (6) (2013) 065004–065012.
[23] S. Tol, F.L. Degertekin, A. Erturk, Gradient-index phononic crystal lens-based enhancement of elastic wave energy harvesting, Appl. Phys. Lett. 109 (6) (2016) 063902.
[24] K. Yi, M. Collet, M. Ichchou, L. Li, Flexural waves focusing through shunted piezoelectric patches, Smart Mater. Struct. 25 (7) (2016) 075007.
[25] Tsung Tsong Wu, Yan Ting Chen, Jia Hong Sun, Sz Chin Steven Lin, Tony Jun Huang, Focusing of the lowest antisymmetric Lamb wave in a gradient-index phononic crystal plate, Appl. Phys. Lett. 98 (17) (2011) 171911.
[26] J.N. Reddy, Mechanics of Laminated Composite Plates and Shells: Theory and Analysis, second ed., CRC Press, New York, London, 2004.
[27] Hao Zhang, Jihong Wen, Yong Xiao, Gang Wang, Xisen Wen, Sound transmission loss of metamaterial thin plates with periodic subwavelength arrays of shunted piezoelectric patches, J. Sound Vib. 343 (2015) 104–120.
[28] Steven R. Anton, Henry A. Sodano, A review of power harvesting using piezoelectric materials (2003–2006), Smart Mater. Struct. 16 (3) (2007) R1–R21.
[29] Jens Becker, Oliver Fein, Matthias Maess, Lothar Gaul, Finite element-based analysis of shunted piezoelectric structures for vibration damping, Comput. Struct. 84 (31–32) (2006) 2340–2350.
[30] Ushnish Basu, Anil K. Chopra, Perfectly matched layers for time-harmonic elastodynamics of unbounded domains: theory and finite-element implementation, Comput. Methods Appl. Mech. Eng. 192 (11) (2003) 1337–1375.
[31] Karl F. Graff, Wave Motion in Elastic Solids, Courier Corporation, 2012.
[32] Benjamin S. Beck, Kenneth A. Cunefare, Manuel Collet, The power output and efficiency of a negative capacitance shunt for vibration control of a flexural system, Smart Mater. Struct. 22 (6) (2013) 065009.